

# DFT Case Study on the Comparison of Ruthenium-Catalyzed C–H Alkylation, C–H Alkenylation, and Hydroarylation

Lei Zhang,\* Ling-Ling Wang, and De-Cai Fang\*

Cite This: *ACS Omega* 2022, 7, 6133–6141

Read Online

ACCESS |



Metrics &amp; More

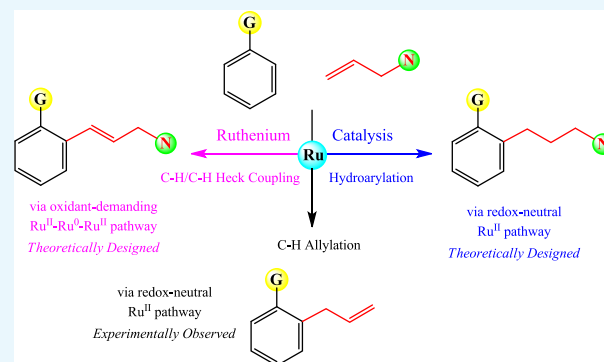


Article Recommendations



Supporting Information

**ABSTRACT:** Density functional calculations at the B3LYP-D3+IDSCRF/TZP-DKH(-dfg) level of theory have been performed to understand the mechanism of ruthenium-catalyzed C–H alkylation reported in the literature in depth. The plausible pathway consisted of four sequential processes, including C–H activation, migratory insertion, amide extrusion, and recovery of the catalyst, in which C–H activation was identified as the rate-determining step. The amide extrusion step could be promoted kinetically by trifluoroacetic acid since its mediation lowered the free-energy barrier from 32.1 to 12.2 kcal/mol. Additional calculations have been performed to explore other common pathways between arenes and alkenes, such as C–H alkenylation and hydroarylation. A comparison of the amide extrusion and  $\beta$ -H elimination steps established the following reactivity sequence of the leaving groups: protonated amide group >  $\beta$ -H group > unprotonated amide group. The suppression of hydroarylation was attributed to the sluggishness of the Ru–C protonation step as compared to the amide extrusion step. This study can unveil factors favoring the C–H alkylation reaction.



## INTRODUCTION

Ruthenium-catalyzed C–H functionalization has drawn particular attention in recent years,<sup>1</sup> among which the dehydrogenative C–C coupling strategy represented a hot issue in modern organometallic chemistry.<sup>2</sup> *Meta*-selective alkylation through  $\sigma$ -activation,<sup>3</sup> the dehydrogenative Heck reaction,<sup>2b,4</sup> direct coupling of two arenes,<sup>5</sup> and dehydrogenative annulation of arenes with alkynes<sup>6</sup> have been regarded as typical examples of ruthenium-catalyzed C–C coupling reactions via C–H activation.

Transition-metal-catalyzed direct coupling of arenes with alkenes provided a powerful and tunable synthetic tool to access the desired skeletons. As two extensively studied reactions in the literature, alkenylation of arenes and hydroarylation of alkenes yielded arylalkenes and arylalkanes, respectively.<sup>7</sup> On the other hand, alkylation of arenes could have been achieved when allyl substrates with a good leaving group were used.

Goossen's group developed several ruthenium-catalyzed alkylation reactions of benzoic acids using some mild allylating reagents, such as allyl acetates, allyl alcohols, allyl ethers, and allyl amines (see Scheme 1a).<sup>8</sup> Scheme 1b shows one of Goossen's previous works, which demonstrated that benzoic acids (**R1**) and allyl amines (**R2**) produced allyl arenes (**P**) under the catalysis of  $[\text{Ru}(p\text{-cymene})\text{Cl}_2]_2$  (*p*-cymene = 4-isopropyltoluene).<sup>8c</sup> These reactions presented the sequential C–H and C–N activations, resulting in the overall C–H alkylation of benzoic acids. Addition of trifluoroacetate (HOTFA) was necessary for furnishing the desired products

in good yields, and trichloroethanol (TCE) was confirmed to be the best solvent. The observed primary kinetic isotopic effects ( $k_{\text{H}}/k_{\text{D}} = 2.8\text{--}4.5$ ) indicated the C–H activation of benzoic acids to be rate-limiting.

Although a number of computational studies on arene–alkene coupling reactions are available in the literature,<sup>9</sup> a comparison of different coupling pathways has rarely been addressed for ruthenium catalysis. With the reaction given in Scheme 1b as a model reaction, we attempt to explore the detailed mechanisms of ruthenium-catalyzed C–H alkylation of benzoic acids by means of density functional theory (DFT) calculations. Moreover, some other coupling pathways between arenes and alkenes will be designed and compared.

## RESULTS AND DISCUSSION

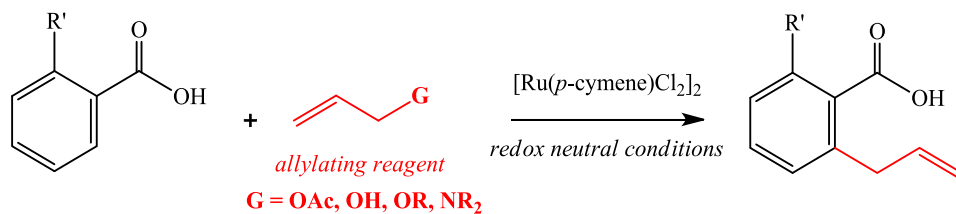
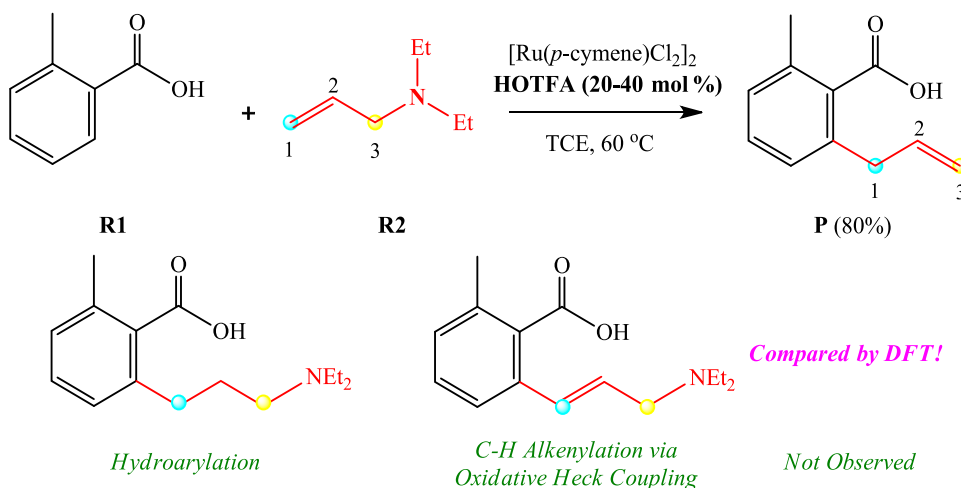
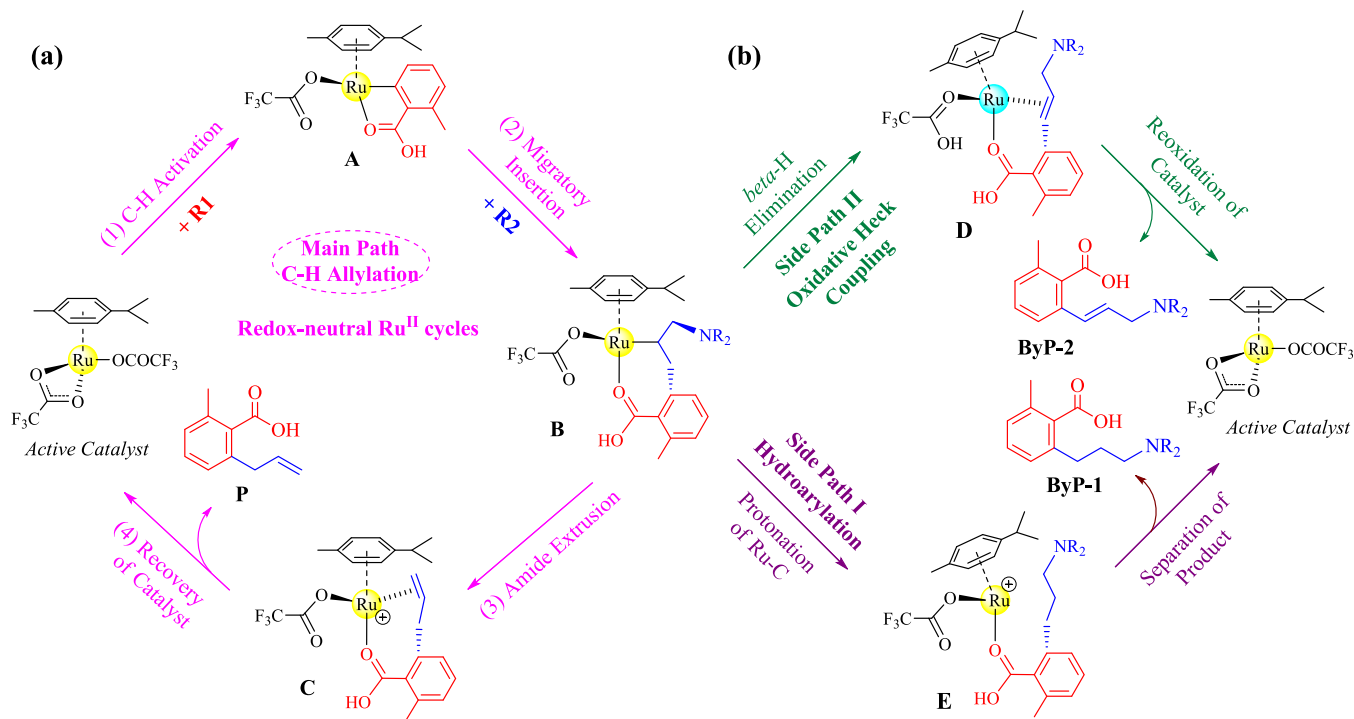
Previous studies disclosed that the binuclear complex  $[\text{RuCl}_2(p\text{-cymene})]_2$  should be able to convert into the mononuclear complex  $\text{Ru}(\text{OAc})_2(p\text{-cymene})$  in the presence of a suitable acetate additive.<sup>10</sup> According to the experimental conditions reported, we have calculated the energetic data associated with

Received: November 22, 2021

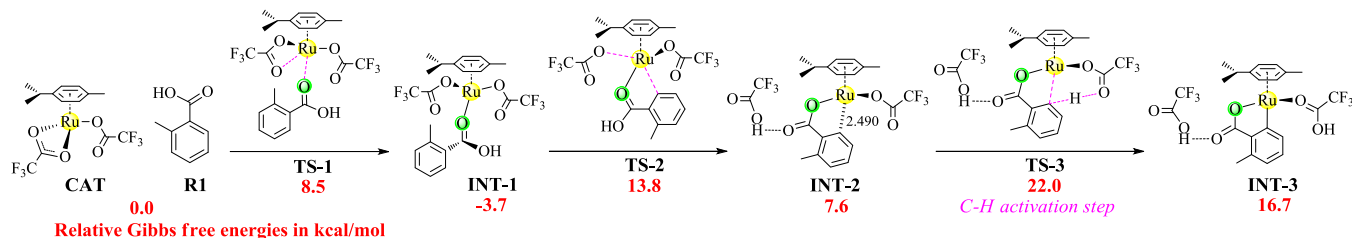
Accepted: January 26, 2022

Published: February 9, 2022

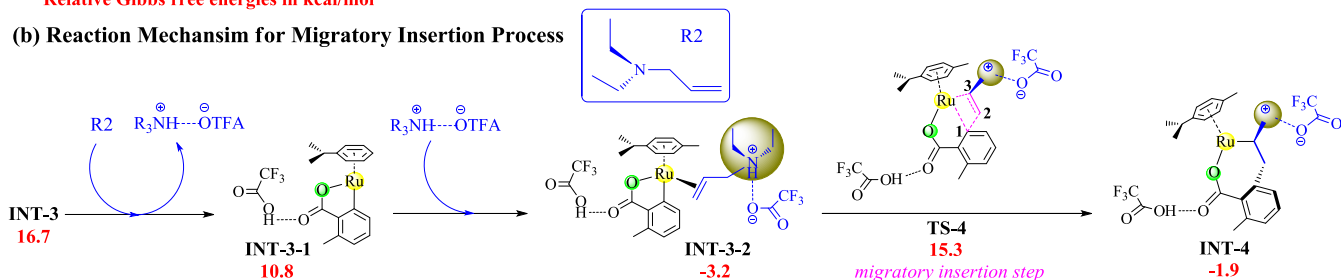


Scheme 1. Ruthenium-Catalyzed C–H Allylation Reactions of Benzoic Acids with Allylating Reagents Studied in This Work by the DFT Method<sup>a</sup>(a) Previous works on ruthenium-catalyzed *ortho* allylation of benzoic acids(b) Ruthenium-catalyzed *ortho* allylation of benzoic acids via C–H/C–N activation<sup>a</sup>(a) C–H allylation using different allylating reagents and (b) C–H allylation via C–H/C–N activation.Scheme 2. Possible Catalytic Pathways for Ruthenium-Catalyzed Cross-Coupling Reactions between Arenes and Alkenes<sup>a</sup><sup>a</sup>(a) C–H allylation and (b) hydroarylation and oxidative Heck coupling.

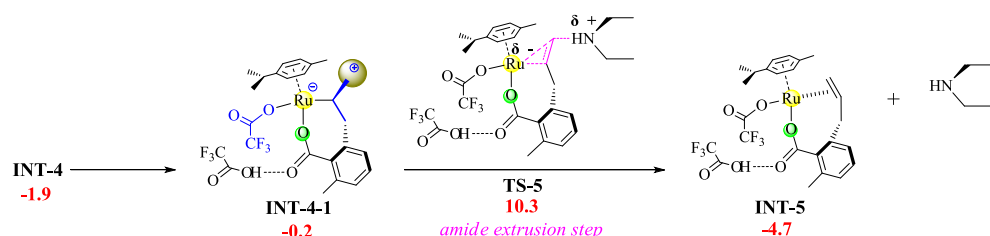
## (a) Reaction Mechanism for C-H Activation Process



## (b) Reaction Mechanism for Migratory Insertion Process



## (c) Reaction Mechanism for Amide Extrusion Process



## (d) Reaction Mechanism for Product Separation and Catalyst Regeneration Processes

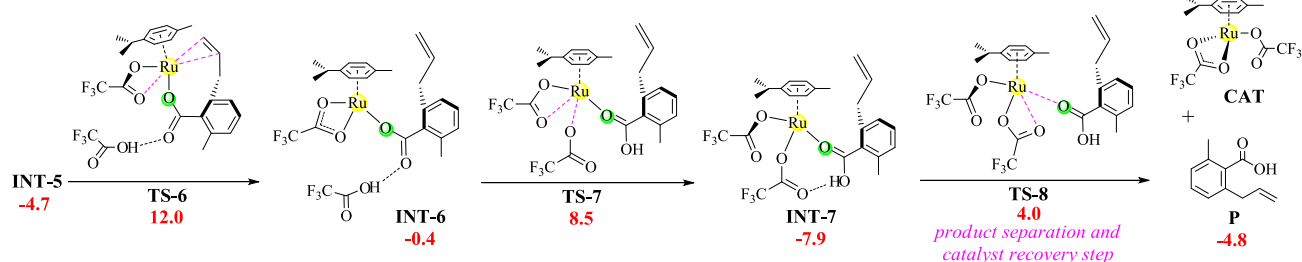


**Figure 1.** Entire reaction pathway for ruthenium-catalyzed C–H allylation between arenes and alkenes, along with the relative free-energy data (in kcal/mol) characterized at the B3LYP-D3+IDSCRF/TZP-DKH(-dft) level of theory. (a) C–H activation, (b) migratory insertion, (c) amide extrusion, and (d) product separation and catalyst regeneration processes.

such a dimer-to-monomer transformation. The chemical equation of  $[\text{RuCl}_2(p\text{-cymene})]_2 + 4 \text{HOTFA} + 4 \text{R2} \rightarrow 2 \text{Ru}(\text{OTFA})_2(p\text{-cymene}) + 4 \text{R2}\cdot\text{HCl}$  was predicted to occur irreversibly, with the total free-energy change of  $-29.9$  kcal/mol at the B3LYP-D3+IDSCRF/TZP-DKH(-dft) level of theory. Additionally, our calculations excluded the possibility of using  $\text{CCl}_3\text{CH}_2\text{O}^-$  (the conjugate base of TCE) as a ligand of central ruthenium because the chemical conversion of  $\text{Ru}(\text{OTFA})_2(p\text{-cymene})$  into  $\text{Ru}(\text{OTFA})(\text{OCH}_2\text{CCl}_3)(p\text{-cymene})$  through the ligand exchange and proton transfer had to absorb free energies of up to 13.1 kcal/mol (see the Supporting Information for details). According to these findings, the assignment of  $\text{Ru}(\text{OTFA})_2(p\text{-cymene})$  as a real catalyst should be reasonable.

The catalytic pathways for the observed C–H allylation reaction and the other two possible reactions are shown in Scheme 2. The catalytic cycle of the main reaction consists of four processes in succession, including C–H activation, migratory insertion, amide extrusion, and recovery of the catalyst and separation of the desired product. The intermediate

**B** resulting from the C–H activation and migratory insertion processes is the branch point of the three pathways. If **B** undergoes protonation of the Ru–C bond instead of amide extrusion, the net hydroarylation of **R2** can be realized through side path I. If the  $\beta$ -H elimination step occurs at **B**, the C–H alkenylation product would be yielded through the typical Heck coupling pathway (side path II). Both the main reaction and side path I are a redox-neutral coupling pathway, while side path II is an oxidative coupling, which would result in catalyst deactivation under oxidant-free conditions. The competition of C–H allylation against these two side reactions is one of the main subjects in this study, and the following discussion is divided into several parts accordingly.

### Mechanism of Ruthenium-Catalyzed C–H Allylation.

The proposed reaction pathway for the observed C–H allylation reaction between **R1** and **R2** is shown in Figure 1. The entry of **R1** into the ligand field of **CAT** results from a ligand-exchange step involving the transition state **TS-1**, in which the carbonyl oxygen of **R1** attacks on the ruthenium center to remove one of

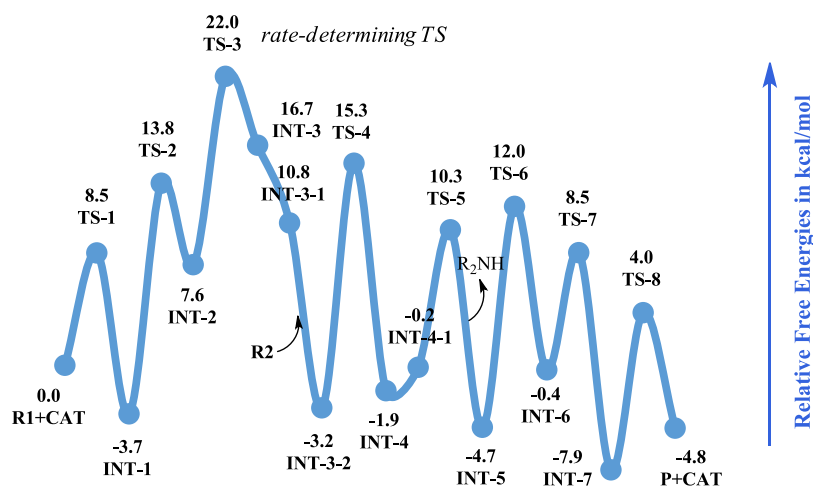


**Figure 2.** Entire free-energy profile (kcal/mol) for the ruthenium-catalyzed C–H allylation reaction calculated at the B3LYP-D3+IDSCRF/TZP-DKH(-dfg) level of theory.

the O-arms of  $\kappa^2$ -OTFA. The encounter intermediate INT-1 undergoes the dissociation of a  $\kappa^1$ -OTFA ligand through the transition state TS-2. The consequent intermediate INT-2 indicates a loose Pd...C interaction with an interatomic distance of 2.490 Å, and the removed  $\kappa^1$ -OTFA group deprotonates the carboxyl group of R1 to form an intermolecular OH...O hydrogen bond. The ligand dissociation from ruthenium should be necessary for the C–H activation step because the ruthenium center of the catalyst is of an  $18e^-$  configuration and forming the target Ru–C bond without the removal of a ligand would violate the effective atomic number rule. Some previous mechanistic studies also suggested that ruthenium-catalyzed C–H activation may involve some charge-separated species as the precursor of proton transfer.<sup>10</sup>

The next step is C–H activation through the transition state TS-3, with the  $\kappa^1$ -OTFA ligand serving as a proton acceptor, which delivers the ruthenacyclic intermediate INT-3. The located C–H activation mechanism is the concerted metalation–deprotonation (CMD) mechanism via a six-center cyclic transition state.<sup>9a</sup> Then, INT-3 undergoes the removal of HOTFA and coordination of ammonium trifluoroacetate, with the latter species being produced from HOTFA and R2. The formed species INT-3-2 is the starting point for the next migratory insertion step.

TS-4 is identified as the transition state of the migratory insertion step and has the typical four-center cyclic structure, in which the bond formation of C1–C2 and Ru–C3 and the bond cleavage of Ru–C1 take place in a concerted manner. The consequent intermediate INT-4 is a seven-member ruthenacyclic species, from which the OTFA group bonded to the ammonium hydrogen can coordinate to ruthenium, giving a different intermediate INT-4-1. The amide extrusion step from INT-4-1 is required to pass over the transition state TS-5, removing the neutral amine  $(C_2H_5)_2NH$  and delivering the double bond in a concerted manner. The product exists as a bidentate ligand in INT-5.

The double bond of the product may dissociate from ruthenium through an intramolecular ligand exchange via the transition state TS-6, causing the change of  $\kappa^1$ -OTFA to  $\kappa^2$ -OTFA. However, the removal of the product carbonyl oxygen from ruthenium may be achieved by two ligand exchange steps. First, the OTFA group hydrogen-bonded to the product moiety coordinates to ruthenium via the transition state TS-7, changing

the  $\kappa^2$ -OTFA ligand in INT-6 to the  $\kappa^1$ -OTFA ligand in INT-7. Then, the ligand exchange via the transition state TS-8 can release the product P and regenerate the active catalyst CAT. We failed to locate a one-step substitution process linking INT-6 to P+CAT. It is worth noting that the ruthenium center retains the oxidation state of +2 throughout the entire catalytic cycle, indicating a redox-neutral C–H/C–N coupling reaction performed under oxidant-free conditions.

The free-energy alterations along the proposed pathway are shown in Figure 2. The combination of CAT and R1 is moderately favored by a free energy of 3.7 kcal/mol. The dissociation of  $\kappa^1$ -OTFA is required to overcome a free-energy barrier of 17.5 kcal/mol (TS-2) and absorb free energies of up to 11.3 kcal/mol. The rate-determining transition state is identified to be TS-3 in the C–H activation step, which lies at 25.7 kcal/mol, in free energy, above INT-1. On this basis, the kinetic isotope  $k_H/k_D$  value is computed to be 4.53, close to the experimental value (2.8–4.5).<sup>8c</sup> Although INT-3 is quite unstable with a free energy of 16.7 kcal/mol, it can evolve to the stable species INT-3-2 by releasing free energies of 3.2 kcal/mol. The migratory insertion process involves a free-energy barrier of 18.5 kcal/mol and generates a slightly stable intermediate (INT-4-1). The free-energy barrier of the amide extrusion step via TS-5 is merely 12.2 kcal/mol, and then, free energies of 4.7 kcal/mol are liberated. The separation of the product does not involve a very high-lying transition structure, and the whole reaction is exothermic with a free energy of 4.8 kcal/mol.

As the C–H activation step is rate-determining, we have located some other transition states for scissoring the target C–H bond. The proton-transfer transition state using amine R2 as an external base involves a total free-energy barrier of 30.1 kcal/mol. The proton-transfer transition state using the hydrogen-bonded OTFA anion as an external base suffers from a much higher free-energy barrier. The detailed geometries and energetic data are provided in the Supporting Information. Such external-base-induced C–H activation processes resemble the electrophilic deprotonation–metallation mechanism. These data suggest that the CMD mechanism should be more plausible for the present C–H activation step.

In addition, experimental researchers<sup>8c</sup> have put forward a different pathway, in which INT-3-2 may undergo the direct removal of the amide group rather than the migratory insertion

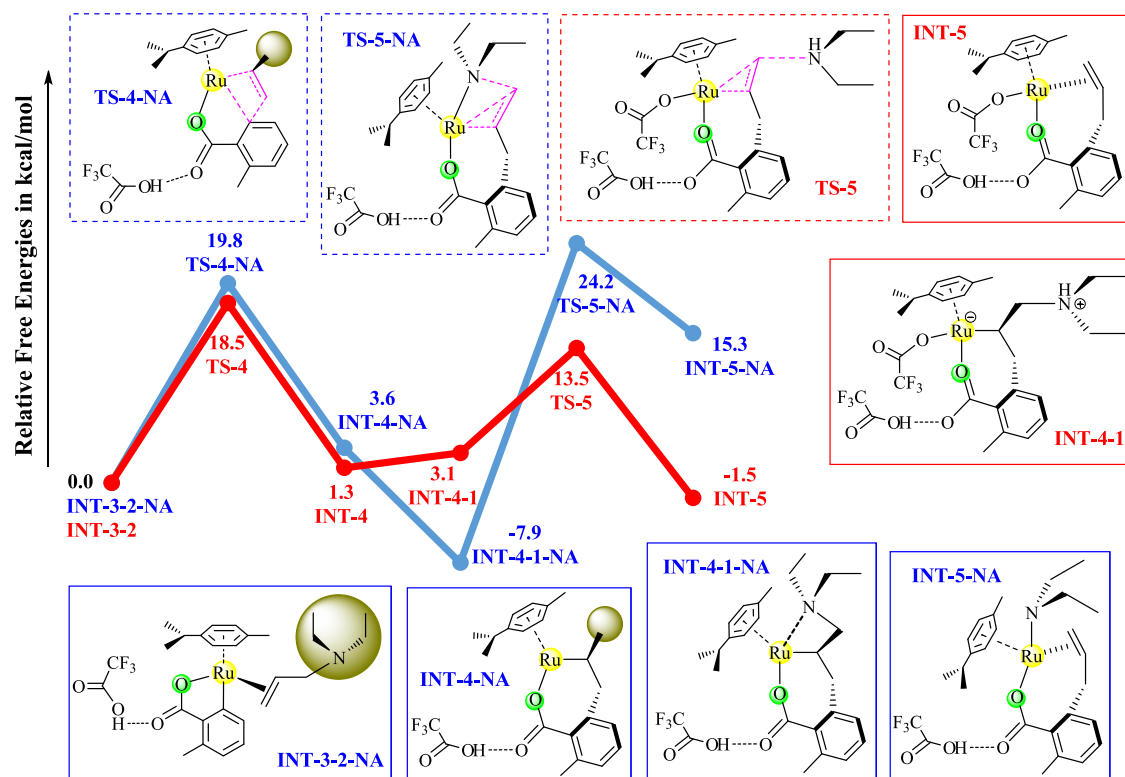


**Figure 3.** Migratory insertion and amide extrusion processes (in blue) without the assistance of HOTFA, that is, R2 instead of R2+HOTFA engages in the reaction. Free-energy data are determined at the B3LYP-D3+IDSCRF/TZP-DKH(-d3g) level of theory. The favorable pathway (in red) is comparatively shown.

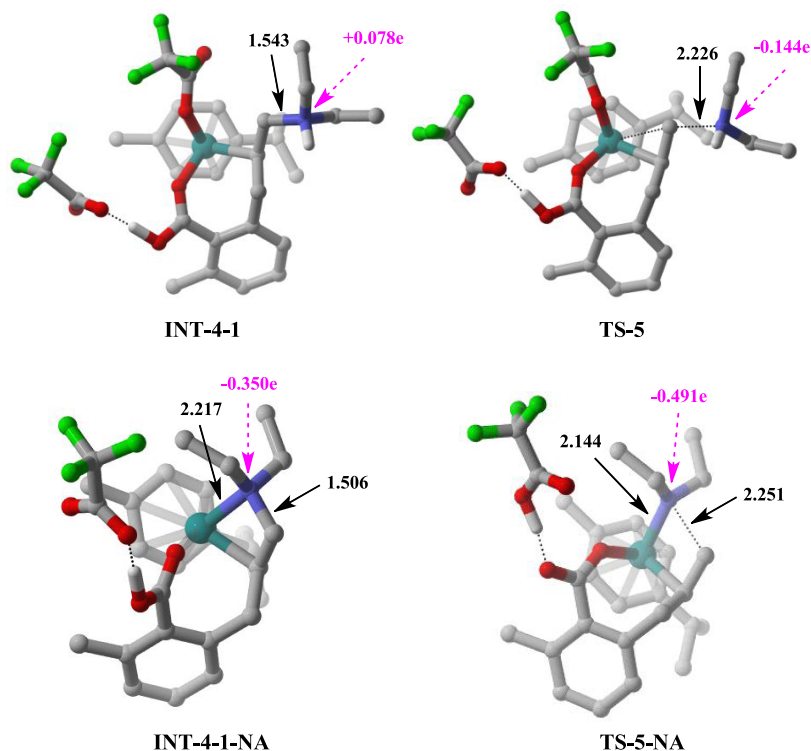


**Figure 4.** Three-dimensional structures involved in the amide extrusion processes, with the selected bond-length values (in black, Å) and NBO charge values (in pink, e). Hydrogen atoms on the carbon centers are all omitted for the sake of simplicity.

step. This mechanistic proposal supposed the formation of a ruthenium-( $\eta^3$ -allyl) complex and could be ruled out by our calculations (see the Supporting Information).

**Role of HOTFA in Promoting Amide Extrusion.** The mechanism of the amide extrusion step in Figure 1 reflects the crucial role of HOTFA because the protonation by HOTFA can

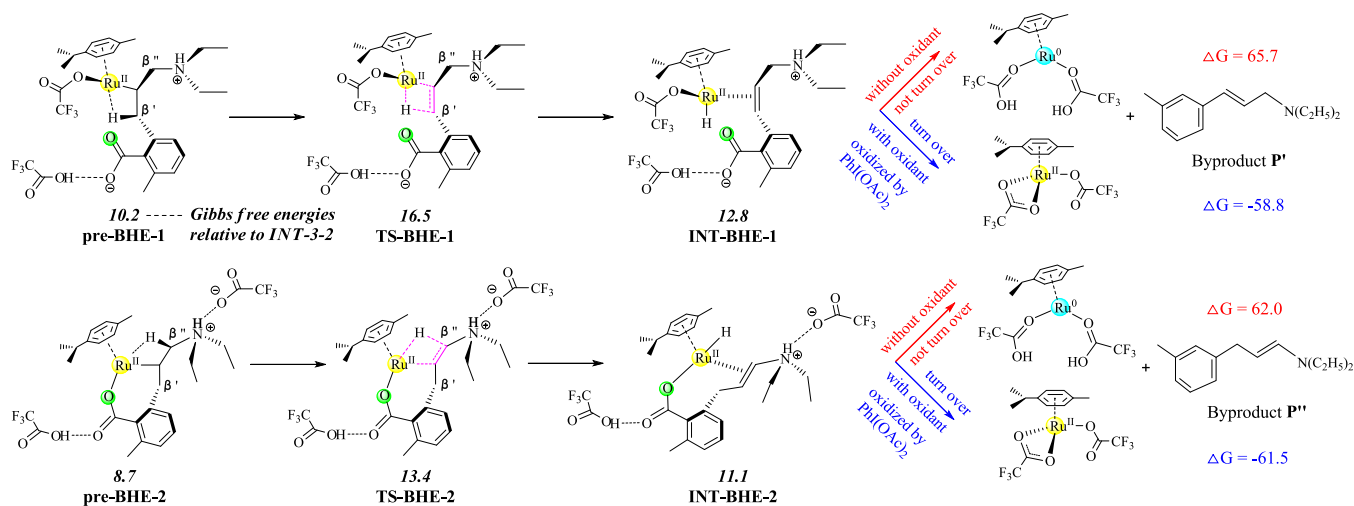


**Figure 5.** Designed  $\beta$ -H elimination processes and the corresponding free-energy values (in kcal/mol) calculated at the B3LYP-D3+IDSCRF/TZP-DKH(-dfg) level of theory.

significantly enhance the leaving group ability by transforming a neutral amine into cationic ammonium. To analyze the effect of HOTFA on the mechanism and energetics, we theoretically design a reaction channel without the assistance of HOTFA, in which the amide group is unprotonated upon elimination. This mechanistic proposal should be considered because the amount of **R2** is much larger than that of HOTFA. The reaction pathway shown in Figure 3 (in blue) depicts the scene in which **R2**, rather than species **R2**+HOTFA, coordinates to the ruthenium center of INT-3-1 and engages in the migratory insertion and subsequent steps. In this case, the amide group might not be removed directly from INT-4-NA because this would generate a bivalent nitrogen species that should be highly unstable. The formation of a Ru–N dative bond is a requisite prior to the removal of the amide group because the energy cost of the C–N bond cleavage may be compensated by the strengthening of the Ru–N interaction in TS-5-NA (Ru–N distance: 2.217 Å in INT-4-1-NA and 2.144 Å in TS-5-NA). This process can overcome a very high free-energy barrier of 32.1 kcal/mol and absorb free energies of 15.3 kcal/mol, which undoubtedly rule out it as an accessible pathway at 60 °C.

For comparison, Figure 3 (in red) also provides the favorable pathway with **R2**+HOTFA as the reagent, as discussed earlier. It mainly benefits from a much lower free-energy barrier of the amide extrusion step via TS-5. The optimized structures of INT-4-1 and TS-5 in Figure 4 show that the target C–N bond lengthens from 1.543 to 2.226 Å, while it lengthens from 1.506 Å in INT-4-1-NA to 2.251 Å in TS-5-NA, indicating that the removal of the protonated amide group is relatively more favorable. Additionally, natural bond orbital (NBO) charges at the selected atoms are shown in Figure 4. The NBO charge value at the nitrogen atom changes from +0.078 e in INT-4-1 to –0.144 e in TS-5, supporting the enhanced reactivity of the positively charged ammonium group.

On the basis of DFT calculations, HOTFA indeed plays a key role in facilitating the amide extrusion step because the protonation by HOTFA transforms the neutral amine into the more labile ammonium. In contrast, the direct removal of the amide group without the assistance of HOTFA is required to overcome a much higher free-energy barrier.

**Competition of the  $\beta$ -H Elimination Reaction.** After migratory insertion, the  $\beta$ -H elimination step leading to the C–

H alkenylation of **R1** is also a common reaction mode, which is different from the amide extrusion step leading to the observed C–H allylation of **R1**. As the terminal step in traditional Heck couplings, the  $\beta$ -H elimination step generally forms an olefinic bond through a hydrogen shift from  $\beta$ -carbon to metal. To make clear the factors favoring the amide extrusion over  $\beta$ -H elimination, we theoretically design some  $\beta$ -H elimination steps after migratory insertion. Judging from the geometries of INT-4 and INT-4-1, the  $\beta$ -H elimination step may occur at either of two positions ( $\beta'$  or  $\beta''$ ), which lead to different alkenylation byproducts (**P'** and **P''**). Figure 5 shows the optimized transition states for eliminating  $\beta'$ -H or  $\beta''$ -H, respectively, from which one can see that the hydrogen atom is abstracted by the ruthenium center involving a four-center transition state (TS-BHE-1 or TS-BHE-2). Subsequently, a ruthenium-hydride complex (INT-BHE-1 or INT-BHE-2) with a byproduct moiety is produced. Computational data reveal that the free-energy barriers of the  $\beta$ -H elimination steps are in a range of 13.4–16.5 kcal/mol, which should be kinetically accessible at the experimental temperature.

Comparatively, the free-energy barriers of the  $\beta$ -H elimination steps are somewhat higher than that (12.2 kcal/mol) of the amide extrusion step with the promotion of HOTFA, but they are much lower than that (32.1 kcal/mol) of the amide extrusion step without the promotion of HOTFA. The following reactivity sequence of the leaving groups is established in the field of ruthenium catalysis according to the computational results: protonated amide group >  $\beta$ -H group > unprotonated amide group with the help of ruthenium.

In fact, C–H alkenylation reactions via C–H/C–H coupling require the use of stoichiometric oxidants for the regeneration of the active catalyst. Under oxidant-free conditions, both of the C–H alkenylation reactions shown in Figure 5 can not turn over because the production of **P'** or **P''**, with a Ru(0) complex, absorbs free energies by as much as 65.7 or 62.0 kcal/mol. The catalytic reaction may become spontaneous in the presence of a suitable oxidant. It is predicted that employing iodobenzene diacetate  $\text{PhI}(\text{OAc})_2$  as the terminal oxidant leads to strong exothermicity (see Figure 5).

Some predictions beyond the experimental findings can be made. If the reaction is performed under nonacidic conditions,  $\beta$ -H elimination should dominate over the amide extrusion

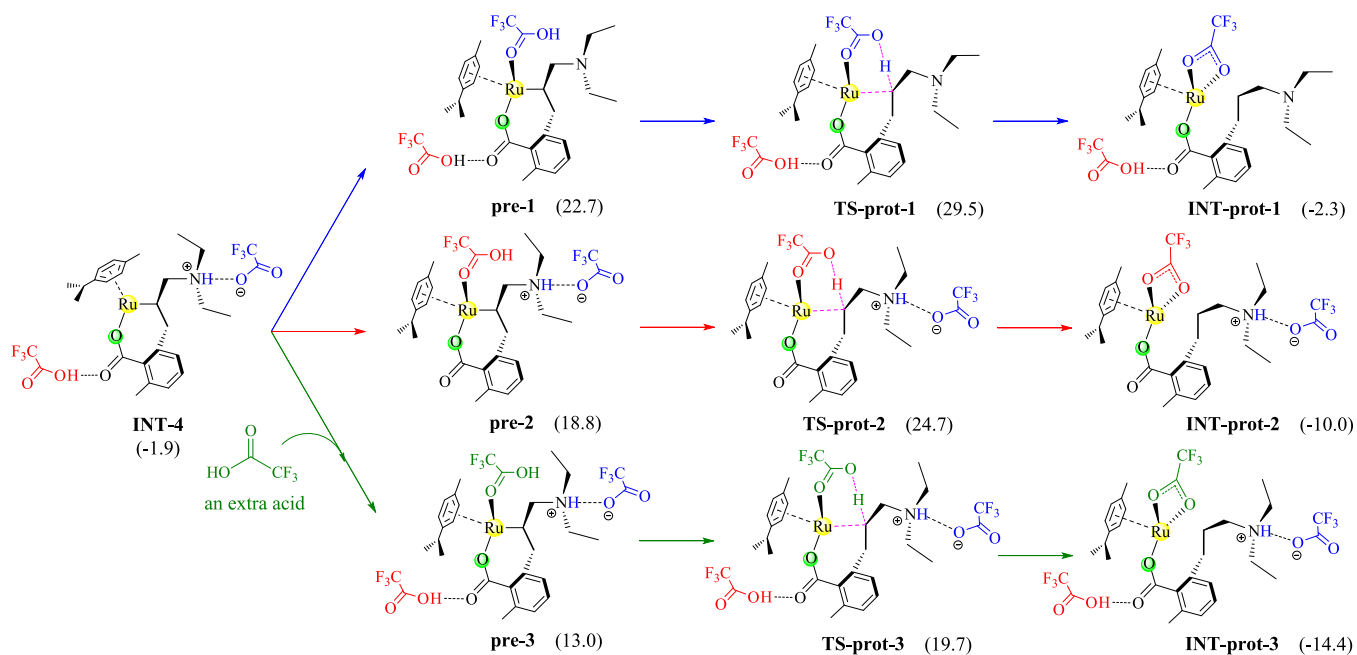


**Figure 6.** Designed protonation–demetalation processes and the corresponding free-energy values (in kcal/mol) calculated at the B3LYP-D3+IDSCRF/TZP-DKH(-d<sub>fg</sub>) level of theory.

kinetically, which might result in catalyst deactivation without an external oxidant. If the reaction is performed under acidic conditions, the amide extrusion process is more competitive than the  $\beta$ -H elimination process, and the latter can be further suppressed using redox-neutral conditions.

**Competition of the Hydroarylation Pathway.** Figure 6 shows the designed pathways for the protonation of the Ru–C bond in INT-4, leading to the hydroarylation of the double bond of R2. To produce the precursor of the protonation step, a molecule of HOTFA needs to serve as a ligand of the ruthenium center. The first two pathways (blue and red) indicate that this HOTFA may be the one hydrogen-bonded to the amide group or the one hydrogen-bonded to the carboxylate group, and precursors **pre-1** and **pre-2** are both highly unstable due to the disconnection of a strong hydrogen bond. The protonation steps via **TS-prot-1** and **TS-prot-2** involve the free-energy barriers of 31.4 and 26.6 kcal/mol, respectively, which are less favorable than those of the main reaction.

On the third pathway (green), the HOTFA ligand is introduced from the external environment, which avoids the rupture of an intramolecular hydrogen-bonding interaction. However, the entropic decrease makes the precursor **pre-3** not stable. Transition state **TS-prot-3** lies at 21.6 kcal/mol above INT-4 and thus is more accessible than those of the former two pathways.

Experimentally, the amount of HOTFA is much smaller than that of R2, which could not meet the requirement of the third pathway and would hinder the protonation of the Ru–C bond kinetically. In addition, the free-energy barrier associated with **TS-prot-3** is still higher than that of the amide extrusion of the main reaction. Therefore, the protonation of the Ru–C bond should be less favorable than the amide extrusion for the present case.

## CONCLUSIONS

A ruthenium-catalyzed C–H allylation reaction was characterized by DFT calculations, in which the plausible mechanism

and the discrimination against other common reaction modes between arenes and alkenes were addressed in great detail. The C–H activation step was identified as the rate-determining step, in line with the kinetic isotopic effects observed experimentally. The removal of the  $\beta$ -group controls the competition of C–H allylation and C–H alkenylation. The amide extrusion, leading to the observed C–H allylation, proceeds favorably with the promotion of HOTFA. The following kinetic sequence of the leaving groups is obtained in the field of ruthenium catalysis: protonated amide group >  $\beta$ -H group > unprotonated amide group. The suppression of the hydroarylation pathway is mainly due to the kinetic sluggishness of the Ru–C protonation process because of the energy cost involved in the cleavage of the favorable intramolecular interactions.

## COMPUTATIONAL DETAILS

Calculations were performed using the B3LYP density functional method<sup>11</sup> in the Gaussian 09 program package.<sup>12</sup> To balance the computational cost and accuracy, the TZP-DKH(-d<sub>fg</sub>) basis sets, originated from TZP-DKH basis sets<sup>13</sup> via the removal of *d* functions from H atoms, *f* functions from C, O, N, and F atoms, and *g* functions from a Ru atom, have been employed in all calculations. The default self-consistent reaction field polarizable continuum model<sup>14</sup> was employed to mimic the solvation effect, in which our IDSCRF radii<sup>15</sup> were chosen to define the molecular space. In the present computational study, trifluoroethanol was used as a solvent instead of trichloroethanol since the latter solvent was unavailable in the Gaussian 09 program. The dispersion contribution was considered by Grimme's D3(BJ) method<sup>16</sup> in both geometrical optimizations and energetic determinations. All of the optimized stationary points were subjected to vibrational analyses to obtain zero-point energies and entropies for Gibbs free-energy calculations and ensure that they were minima or first-order saddle points (transition states) on the potential energy surfaces. The three-dimensional molecular geometries were illustrated using CYLVIEW software.<sup>17</sup>

The default translational entropies computed by the Gaussian 09 program are ideal-gas-phase translational entropies, which would exaggerate the entropy decrease of bimolecular reactions in solution.<sup>18</sup> In the present study, our solution translational entropy model encoded in the THERMO program<sup>19</sup> was used to compute more accurate entropic and free-energy data. Such a solution translational entropy model has previously been applied to Gibbs free-energy calculations in solution.<sup>20</sup>

## ASSOCIATED CONTENT

### Supporting Information

The Supporting Information is available free of charge at <https://pubs.acs.org/doi/10.1021/acsomega.1c06584>.

Optimized geometric parameters for all stationary points; imaginary frequencies of all transition states; electronic energies, zero-point energies, and total free energies; and complementary mechanistic characterization (PDF)

## AUTHOR INFORMATION

### Corresponding Authors

Lei Zhang – School of Science, Tianjin Chengjian University, Tianjin 300384, P. R. China; [orcid.org/0000-0003-0100-8357](https://orcid.org/0000-0003-0100-8357); Email: [zhanglei-chem@tcu.edu.cn](mailto:zhanglei-chem@tcu.edu.cn)

De-Cai Fang – College of Chemistry, Beijing Normal University, Beijing 100875, P. R. China; [orcid.org/0000-0003-3922-7221](https://orcid.org/0000-0003-3922-7221); Email: [dcfang@bnu.edu.cn](mailto:dcfang@bnu.edu.cn)

### Author

Ling-Ling Wang – School of Science, Tianjin Chengjian University, Tianjin 300384, P. R. China

Complete contact information is available at: <https://pubs.acs.org/doi/10.1021/acsomega.1c06584>

### Notes

The authors declare no competing financial interest.

## ACKNOWLEDGMENTS

This work was supported by the National Natural Science Foundation of China (22003045 and 21773010) and the Fundamental Research Funds for Tianjin Colleges (2018KJ171). L.Z. is grateful for the technical support from the High-Performance Computing Platform of Tianjin Chengjian University.

## REFERENCES

- (1) (a) Molnár, Á.; Papp, A. Ruthenium-catalyzed C–H activation and coupling reactions in organic synthesis. *Curr. Org. Chem.* **2015**, *20*, 381–458. (b) Arockiam, P. B.; Bruneau, C.; Dixneuf, P. H. Ruthenium (II)-catalyzed C–H bond activation and functionalization. *Chem. Rev.* **2012**, *112*, 5879–5918. (c) Ackermann, L. Carboxylate-assisted ruthenium-catalyzed alkyne annulations by C–H/Het–H bond functionalizations. *Acc. Chem. Res.* **2014**, *47*, 281–295. (d) Shan, C.; Zhu, L.; Qu, L.-B.; Bai, R.; Lan, Y. Mechanistic view of Ru-catalyzed C–H bond activation and functionalization: computational advances. *Chem. Soc. Rev.* **2018**, *47*, 7552–7576.
- (2) (a) Yang, Y.; Lan, J.; You, J. Oxidative C–H/C–H coupling reactions between two (hetero)arenes. *Chem. Rev.* **2017**, *117*, 8787–8863. (b) Ma, W.; Gandeepan, P.; Li, J.; Ackermann, L. Recent advances in positional-selective alkenylations: removable guidance for twofold C–H activation. *Org. Chem. Front.* **2017**, *4*, 1435–1467.
- (3) (a) Leitch, J. A.; Frost, C. G. Ruthenium-catalyzed  $\sigma$ -activation for remote meta-selective C–H functionalisation. *Chem. Soc. Rev.* **2017**, *46*, 7145–7153. (b) Yuan, C.; Zhu, L.; Zeng, R.; Lan, Y.; Zhao, Y. Ruthenium(II)-catalyzed C–H difluoromethylation of ketoximes:

tuning the regioselectivity from the meta to the para position. *Angew. Chem., Int. Ed.* **2018**, *57*, 1277–1281. (c) Leitch, J. A.; McMullin, C. L.; Paterson, A. J.; Mahon, M. F.; Bhonoah, Y.; Frost, C. G. Ruthenium-catalyzed para-selective C–H alkylation of aniline derivatives. *Angew. Chem., Int. Ed.* **2017**, *56*, 15131–15135. (d) Wang, X.-G.; Li, Y.; Liu, H.-C.; Zhang, B.-S.; Gou, X.-Y.; Wang, Q.; Ma, J.-W.; Liang, Y.-M. Three-component ruthenium-catalyzed direct meta-selective C–H activation of arenes: a new approach to the alkylation of alkenes. *J. Am. Chem. Soc.* **2019**, *141*, 13914–13922.

(4) (a) Le Bras, J.; Muzart, J. Intermolecular dehydrogenative Heck reactions. *Chem. Rev.* **2011**, *111*, 1170–1214. (b) Kumar, G. S.; Chand, T.; Singh, D.; Kapur, M. Ruthenium-catalyzed C–H functionalization of benzoic acids with allyl alcohols: A controlled reactivity switch between C–H alkenylation and C–H alkylation pathways. *Org. Lett.* **2018**, *20*, 4934–4937. (c) Bakthados, M.; Kumar, P. V. Ruthenium-catalyzed site-selective enone carbonyl directed ortho-C–H activation of aromatics and heteroaromatics with alkenes. *Adv. Synth. Catal.* **2018**, *360*, 2650–2658. (d) Manikandan, R.; Jeganmohan, M. Recent advances in the ruthenium(II)-catalyzed chelation-assisted C–H olefination of substituted aromatics, alkenes and heteroaromatics with alkenes via the deprotonation pathway. *Chem. Commun.* **2017**, *53*, 8931–8947. (e) Das, R.; Khot, N. P.; Deshpande, A. S.; Kapur, M. Catalyst control in switching the site selectivity of C–H olefinations of 1,2-dihydroquinolines: An approach to positional-selective functionalization of quinolines. *Chem. – Eur. J.* **2020**, *26*, 927–938.

(5) (a) Simonetti, M.; Perry, G. J. P.; Cambeiro, X. C.; Juliá-Hernández, F.; Arokianathar, J. N.; Larrosa, I. Ru-catalyzed C–H arylation of fluoroarenes with aryl halides. *J. Am. Chem. Soc.* **2016**, *138*, 3596–3606. (b) Chinnagolla, R. K.; Jeganmohan, M. Ruthenium-catalyzed ortho-arylation of acetanilides with aromatic boronic acids: an easy route to prepare phenanthridines and carbazoles. *Chem. Commun.* **2014**, *50*, 2442–2444. (c) Dana, S.; Chowdhury, D.; Mandal, A.; Chipem, F. A. S.; Baidya, M. Ruthenium(II) catalysis/noncovalent interaction synergy for cross-dehydrogenative coupling of arene carboxylic acids. *ACS Catal.* **2018**, *8*, 10173–10179. (d) Nareddy, P.; Jordan, F.; Szostak, M. Recent developments in ruthenium-catalyzed C–H arylation: Array of mechanistic manifolds. *ACS Catal.* **2017**, *7*, 5721–5745. (e) Wilkinson, L. A.; Pike, J. A.; Walton, J. W. C–H Activation of  $\pi$ -arene ruthenium complexes. *Organometallics* **2017**, *36*, 4376–4381. (f) Rogge, T.; Ackermann, L. Arene-Free Ruthenium(II/IV)-Catalyzed Bifurcated Arylation for Oxidative C–H/C–H Functionalizations. *Angew. Chem., Int. Ed.* **2019**, *58*, 15640–15645.

(6) (a) Wu, X.-W.; Wang, B.; Zhou, S.-B.; Zhou, Y.; Liu, H. Ruthenium-catalyzed redox-neutral [4+1] annulation of benzamides and propargyl alcohols via C–H bond activation. *ACS Catal.* **2017**, *7*, 2494–2499. (b) Warratz, S.; Kornhaas, C.; Cajaraville, A.; Niepötter, B.; Stalke, D.; Ackermann, L. Ruthenium(II)-catalyzed C–H activation/alkyne annulation by weak coordination with O<sub>2</sub> as the sole oxidant. *Angew. Chem., Int. Ed.* **2015**, *54*, 5513–5517.

(7) (a) Zhang, L.; Fang, D.-C. DFT studies on the directing group dependent arene–alkene cross-couplings: arene activation vs. alkene activation. *Org. Biomol. Chem.* **2015**, *13*, 7950–7960. (b) Zhang, L.; Jiang, B.; Chen, Y.; Lv, J.-F.; Feng, W.-C. A computational study on the reaction mechanisms of nickel-catalyzed diarylation of alkenes. *Eur. J. Org. Chem.* **2019**, *2019*, 6217–6224. (c) Li, Z. Y.; Lakmal, H. H. C.; Qian, X.; Zhu, Z.; Donnadiou, B.; McClain, S. J.; Xu, X.; Cui, X. Ruthenium-catalyzed enantioselective C–H functionalization: A practical access to optically active indoline derivatives. *J. Am. Chem. Soc.* **2019**, *141*, 15730–15736. (d) Li, G.; Liu, Q.; Vasamsetty, L.; Guo, W.; Wang, J. Ruthenium(II)-catalyzed asymmetric inert C–H bond activation assisted by a chiral transient directing group. *Angew. Chem., Int. Ed.* **2020**, *59*, 3475–3479. (e) Matsuura, R.; Jankins, T. C.; Hill, D. E.; Yang, K. S.; Gallego, G. M.; Yang, S.; He, M.; Wang, F.; Marsters, R. P.; McAlpine, I.; Engle, K. M. Palladium(II)-catalyzed  $\gamma$ -selective hydroarylation of alkenyl carbonyl compounds with arylboronic acids. *Chem. Sci.* **2018**, *9*, 8363–8368.

(8) (a) Hu, X.-Q.; Hu, Z.; Trita, A. S.; Zhang, G.; Gooßen, L. J. Carboxylate-directed C–H allylation with allyl alcohols or ethers. *Chem. Sci.* **2018**, *9*, 5289–5294. (b) Trita, A. S.; Biafora, A.; Drapeau,

- M. P.; Weber, P.; Gooßen, L. J. Regiospecific ortho-C–H allylation of benzoic acids. *Angew. Chem., Int. Ed.* **2018**, *57*, 14580–14584. (c) Hu, X.-Q.; Hu, Z.; Zhang, G.; Sivendran, N.; Gooßen, L. Catalytic C–N and C–H bond activation: ortho-allylation of benzoic acids with allyl amines. *Org. Lett.* **2018**, *20*, 4337–4340.
- (9) (a) Zhou, J.; Zhou, Y.; Li, Y.; Zhang, J.; Zhang, L. DFT Mechanistic study on palladium-catalyzed redox-neutral hydroarylation of unactivated alkenes with arylboronic acids. *Asian J. Org. Chem.* **2021**, *10*, 412–420. (b) Shinde, V. S.; Mane, M. V.; Cavallo, L.; Rueping, M. Iridium-catalyzed enantioselective hydroarylation of alkenes through C–H bond activation: experiment and computation. *Chem. – Eur. J.* **2020**, *26*, 8308–8313. (c) Deng, Q.; Li, S.-J.; Wei, D.; Lan, Y. Insights into Lewis base-catalyzed chemoselective [3+2] and [3+4] annulation reactions of MBH carbonates. *Org. Chem. Front.* **2020**, *7*, 1828–1836. (d) Ma, X.-S.; Zhou, Y.; Zhang, L. Theoretical measurements of quantitative effects caused by spectator ligands on palladium-catalyzed C–H activation. *Chin. J. Struct. Chem.*, 2021.
- (10) (a) Flegeau, E. F.; Bruneau, C.; Dixneuf, P. H.; Jutand, A. Autocatalysis for C–H bond activation by ruthenium(II) complexes in catalytic arylation of functional arenes. *J. Am. Chem. Soc.* **2011**, *133*, 10161–10170. (b) Yu, J.-L.; Zhang, S.-Q.; Hong, X. Mechanisms and origins of chemo- and regioselectivities of Ru(II)-catalyzed decarboxylative C–H alkenylation of aryl carboxylic acids with alkynes: a computational study. *J. Am. Chem. Soc.* **2017**, *139*, 7224–7243. (c) Zhang, L.; Yu, L.; Zhou, J.; Chen, Y. Meta-selective C–H alkylation of 2-phenylpyridine catalyzed by ruthenium: DFT study on the mechanism and regioselectivity. *Eur. J. Org. Chem.* **2018**, *2018*, 5268–5277. (d) Ling, B.; Liu, Y.; Jiang, Y.-Y.; Liu, P.; Bi, S. Mechanistic insights into the ruthenium-catalyzed [4+1] annulation of benzamides and propargyl alcohols by DFT studies. *Organometallics* **2019**, *38*, 1877–1886. (e) Lian, B.; Zhang, L.; Fang, D.-C. A computational study on ruthenium-catalyzed [4+1] annulation via C–H activation: the origin of selectivity and the role of the internal oxidizing group. *Org. Chem. Front.* **2019**, *6*, 2600–2606.
- (11) (a) Becke, A. D. Density functional thermochemistry. III The role of exact exchange. *J. Chem. Phys.* **1993**, *98*, 5648–5652. (b) Stephens, P. J.; Devlin, F. J.; Chabalowski, C. F. N.; Frisch, M. J. Ab initio calculation of vibrational absorption and circular dichroism spectra using density functional force fields. *J. Phys. Chem. A* **1994**, *98*, 11623–11627.
- (12) Frisch, M. J.; Trucks, G. W.; Schlegel, H. B.; Scuseria, G. E.; Robb, M. A.; Cheeseman, J. R.; Scalmani, G.; Barone, V.; Mennucci, B.; Petersson, G. A.; Nakatsuji, H.; Caricato, M.; Li, X.; Hratchian, H. P.; Izmaylov, A. F.; Bloino, J.; Zheng, G.; Sonnenberg, J. L.; Hada, M.; Ehara, M.; Toyota, K.; Fukuda, R.; Hasegawa, J.; Ishida, M.; Nakajima, T.; Honda, Y.; Kitao, O.; Nakai, H.; Vreven, T.; Montgomery, J. A., Jr.; Peralta, J. E.; Ogliaro, F.; Bearpark, M.; Heyd, J. J.; Brothers, E.; Kudin, K. N.; Staroverov, V. N.; Kobayashi, R.; Normand, J.; Raghavachari, K.; Rendell, A.; Burant, J. C.; Iyengar, S. S.; Tomasi, J.; Cossi, M.; Rega, N.; Millam, J. M.; Klene, M.; Knox, J. E.; Cross, J. B.; Bakken, V.; Adamo, C.; Jaramillo, J.; Gomperts, R.; Stratmann, R. E.; Yazyev, O.; Austin, A. J.; Cammi, R.; Pomelli, C.; Ochterski, J. W.; Martin, R. L.; Morokuma, K.; Zakrzewski, V. G.; Voth, G. A.; Salvador, P.; Dannenberg, J. J.; Dapprich, S.; Daniels, A. D.; Farkas, O.; Foresman, J. B.; Ortiz, J. V.; Cioslowski, J.; Fox, D. J. *Gaussian 09, revision A.02*; Gaussian, Inc.: Wallingford, CT, 2009.
- (13) (a) Jorge, F. E.; Canal Neto, A.; Camiletti, G. G.; Machado, S. F. Contracted Gaussian basis sets for Douglas–Kroll–Hess calculations: Estimating scalar relativistic effects of some atomic and molecular properties. *J. Chem. Phys.* **2009**, *130*, No. 064108. (b) Campos, C. T.; Jorge, F. E. Triple zeta quality basis sets for atoms Rb through Xe: Application in CCSD(T) atomic and molecular property calculations. *Mol. Phys.* **2013**, *111*, 167–173.
- (14) Scalmani, G.; Frisch, M. J. Continuous surface charge polarizable continuum models of solvation. I. General formalism. *J. Chem. Phys.* **2010**, *132*, No. 114110.
- (15) (a) Tao, J. Y.; Mu, W. H.; Chass, G. A.; Tang, T. H.; Fang, D.-C. Balancing the atomic waistline: Isodensity-based scrf radii for main-group elements and transition metals. *Int. J. Quantum Chem.* **2013**, *113*, 975–984. (b) Fang, D.-C. *SCRFRADII Program*; Beijing Normal University: Beijing, China, 2013.
- (16) (a) Grimme, S. Semiempirical GGA-type density functional constructed with a long-range dispersion correction. *J. Comput. Chem.* **2006**, *27*, 1787–1799. (b) Grimme, S.; Antony, J.; Ehrlich, S.; Krieg, H. A consistent and accurate ab initio parametrization of density functional dispersion correction (DFT-D) for the 94 elements H–Pu. *J. Chem. Phys.* **2010**, *132*, No. 154104.
- (17) Legault, C. Y. *CYLView, 1.0b*; Université de Sherbrooke: Canada, 2009.
- (18) (a) Mammen, M.; Shakhnovich, E. I.; Deutch, J. M.; Whitesides, G. M. Estimating the entropic cost of self-assembly of multiparticle hydrogen-bonded aggregates based on the cyanuric acid melamine lattice. *J. Org. Chem.* **1998**, *63*, 3821–3830. (b) Besora, M.; Vidossich, P.; Lledós, A.; Ujaque, G.; Maseras, F. Calculation of reaction free energies in solution: A comparison of current approaches. *J. Phys. Chem. A* **2018**, *122*, 1392–1399.
- (19) Fang, D.-C. *THERMO Program*; Beijing Normal University: Beijing, China, 2013.
- (20) (a) Han, L.-L.; Li, S.-J.; Fang, D.-C. Theoretical estimation of kinetic parameters for nucleophilic substitution reactions in solution: an application of a solution translational entropy model. *Phys. Chem. Chem. Phys.* **2016**, *18*, 6182–6190. (b) Li, S.-J.; Fang, D.-C. A DFT kinetic study on 1, 3-dipolar cycloaddition reactions in solution. *Phys. Chem. Chem. Phys.* **2016**, *18*, 30815–30823. (c) Zhang, L.; Fang, D.-C. Key role of PdIV intermediates in promoting PdII-catalyzed dehydrogenative homocoupling of two arenes: A DFT study. *Organometallics* **2017**, *36*, 4943–4951. (d) Zhang, L.; Fang, D.-C. Explicit roles of diverse directing groups in determining transition state energy and reaction exothermicity of C–H activation pathways. *Org. Chem. Front.* **2017**, *4*, 1250–1260. (e) Zhang, L.-L.; Zhang, L.; Li, S.-J.; Fang, D.-C. DFT studies on the distinct mechanisms of C–H activation and oxidation reactions mediated by mononuclear- and binuclear-palladium. *Dalton Trans.* **2018**, *47*, 6102–6111.